Journal of Materials Chemistry A

H- and J-Aggregation Inspiring Efficient Solar Conversion

Journal:	*Journal of Materials Chemistry A*
Manuscript ID	TA-ART-11-2020-011146
Article Type:	Paper
Date Submitted by the Author:	16-Nov-2020
Complete List of Authors:	Zhao, Qiaoqiao; Southern University of Science and Technology, Chemistry Lai, Hanjian; Southern University of Science and Technology, Chemistry Chen, Hui; South University of Science and Technology of China, Chemistry Li, Heng; Southern University of Science and Technology, Chemistry He, Feng; Southern University of Science and Technology, Chemistry

H- and J-Aggregation Inspiring Efficient Solar Conversion

Qiaoqiao Zhao [‡a,b], *Hanjian Lai* [‡a], *Hui Chen* [a], *Heng Li* [a], *Feng He* [*a,c]

[a] Shenzhen Grubbs Institute and Department of Chemistry, Southern University of Science and Technology, Shenzhen 518055, China

[b] State Key Laboratory of Biobased Material and Green Papermaking, Qilu University of Technology, Shandong Academy of Sciences, Jinan 250353, China

[c] Guangdong Provincial Key Laboratory of Catalysis, Southern University of Science and Technology, Shenzhen 518055, China

‡ The authors contributed equally to this work.

*E-mail: hef@sustech.edu.cn (F.H.)

Table of Contents

Control H- and J-aggregation of non-fullerene acceptor and research their different influence on photovoltaic performance.

Abstract

Studies of morphology of organic solar cells (OSC) in bulk heterojunction (BHJ) structures are usually focussed on nanoscale morphology. However, morphology at molecular level, such as aggregation type, may also have a profound influence on the performance of OSCs. It is found that H- and J-aggregation coexist in BTIC-CF_3-m and can be easily controlled by different additives. This provides a chance to study and gain a deeper insight into the role of the two aggregation types by directly comparing their effect on various photovoltaic performance parameters. Two common additives, 1-chloronaphthalene (CN) and 1,8-diiodooctane (DIO), support the formation of H- and J-aggregation, respectively and have different effects on the photovoltaic performance of OSCs. H-aggregation favors a higher open circuit voltage (V_{oc}), while J-aggregation favors a higher short circuit current (J_{sc}). Both of these aggregation types can improve the fill factor (FF). On the whole, both the improvement of H- and J-aggregation can enhance the power conversion efficiency (PCE) and the H-aggregation of BTIC-CF_3-m is more efficient in the system of PBDB-TF:BTIC-CF_3-m. Then, H- and J-aggregation are further tuned by solvent vapor annealing (SVA), and consequently the PCE is enhanced to 16.36% from its pristine value of 13.37%. It demonstrates that the morphology optimization, especially precise control of the H- and J-aggregations, is the key factor to further improving premium organic solar conversion systems.

Introduction

With the continuing optimization of the chemical structures of donor and acceptor materials and device technology, the power conversion efficiency (PCE) of nonfullerene organic solar cells (NFOSC) has gradually increased.[1-6] Excellent light absorption performance and easily adjustable energy levels and band gaps of nonfullerene acceptors allow full utilization of solar energy and match better with donors, and as a result, many NFOSCs with outstanding PCEs have been produced.[3-4, 7-10]

In addition to the chemical structures of donors and acceptors and the nanoscale morphology of the active layer, the molecular aggregation type in the active layer is also important in the performance of OSCs,[11-14] although relative studies, especially in-depth research efforts are rare. H- and J-aggregation are two common modes of stacking of conjugated molecules,[15-19] and are formed through the π–π interactions between the conjugated units.[20] Adjacent conjugated units stack face-to-face to form H-aggregation, and head-to-tail to form J-aggregation.[16, 21] H- and J-aggregation depend on the angle between the conjugated plane and the aggregation direction. If the angle is above the theoretical value of 54.7°, H-aggregation is usually observed, while in J-aggregates an angle below 54.7° is normal.[22-24] Due to the π–π interactions between adjacent conjugated units, the corresponding lowest excited level becomes a doublet.[20] For H-aggregation, the higher peak corresponds to allowed transitions of H-aggregation, while the lower one corresponds to allowed transitions of

J-aggregation.[25-26] Therefore, the H-aggregation has a higher lowest excited level and the corresponding absorption spectrum is blue-shifted, while J-aggregation has a lower lowest excited level and the corresponding absorption spectrum is red-shifted.[15] From this point, it can be speculated that aggregation behavior will affect the performance of OSCs and the influence of the same aggregation type in materials with different roles, donor or acceptor, will be different. For example, aggregation behavior in donor affect the driving force to dissociate excitons, which is decided by the energy gap between the LUMO energy levels of donor and acceptor. [27] While in acceptor, it can be inferred that the open circuit voltage (V_{oc}), which is determined by the energy gap between the LUMO energy level of acceptor and the HOMO energy level of donor, may be influenced by aggregation behavior. However, the mode and extent of the influence of aggregation type on V_{oc} need to be explored.

In this work, the H- and J-aggregation behavior of acceptor molecules and the resulting influence on the photovoltaic performance were investigated. It was found that H- and J-aggregations coexist in BTIC-CF_3 and they can be easily controlled by different additives. This offers us an opportunity to study systematically and gain a deep insight into the roles of the two aggregation types by directly comparing their effect on various photovoltaic performance parameters. It is found that two common additives, 1-chloronaphthalene (CN) and 1,8-diiodooctane (DIO), are conducive to the formation of H- and J-aggregation, respectively. The aggregation types of the acceptor influence not only J_{sc} but also V_{oc}. H-aggregation favors higher V_{oc} due to its higher lowest excited energy level, while J-aggregation favors higher J_{sc}, because of

the extended absorption range and a lower energy needed for excitation. Both of the two aggregation types could improve the fill factor (FF) as a result of the improved crystallinity. Consequently, both CN and DIO enhance the PCE. However, with DIO as additive, devices had a slightly lower PCE due to the substantial reduction of V_{oc}, resulting from the J-aggregation. Solvent vapor annealing (SVA) was used to futher improve H- and J-aggregation of BTIC-CF_3-m in the blend film PBDB-TF:BTIC-CF_3-m processed by CN. As a result, the PCE was further enhanced from 13.37% in the pristine active layer to 16.36%. From this work, it is clear that tuning H- and J-aggregation is an effective method for targeted regulation of V_{oc} and J_{sc}. This allows us to have a deeper understanding of OSCs and offers us a new targeted way to improve the performance of OSCs.

Results and Discussion

The chemical structures of BTIC-CF_3-m and PBDB-TF are shown in **Figure 1**a and 1b. The synthesis of BTIC-CF_3-m has been reported previously.[28] It is a blend of BTIC-CF_3-γ and BTIC-CF_3-δ, whose chemical structures are shown in **Figure S1**. The mixing ratios of BTIC-CF_3-γ and BTIC-CF_3-δ have an influence on the performance of the devices as shown in **Figure S2** and **Table S1**. Here, BTIC-CF_3-m with 65% BTIC-CF_3-γ was used due to the champion PCE.

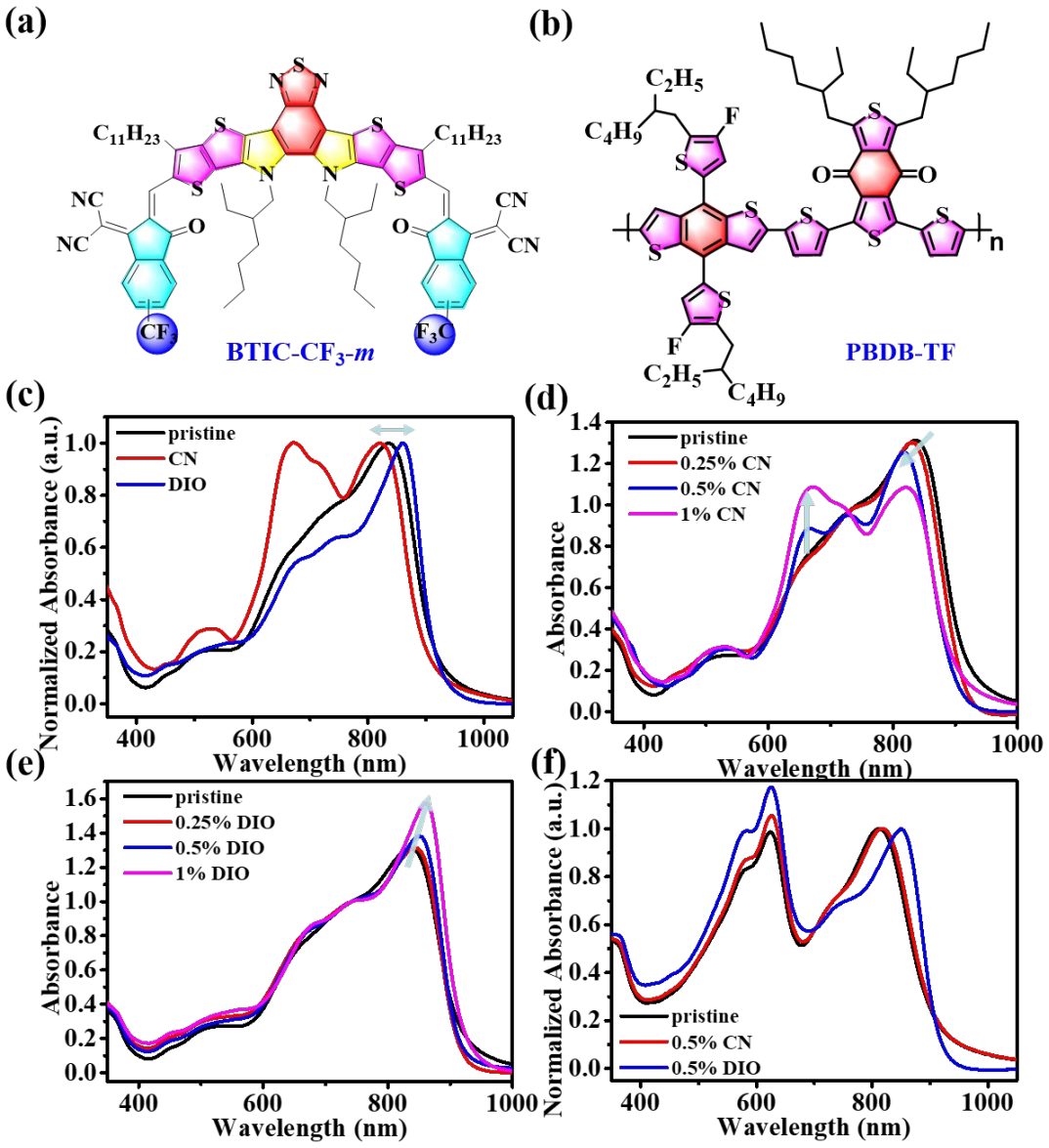

Figure 1. Chemical structures of (a) BTIC-CF_3-m and (b) PBDB-TF; Absorbance of (c) neat BTIC-CF_3-m films without additive and with 1% CN or 1% DIO, (d) neat BTIC-CF_3-m films with different content of CN, (e) neat BTIC-CF_3-m films with different content of DIO and (f) blend films of PBDB-TF:BTIC-CF_3-m without additive and with 1% CN or 1% DIO.

It is found that the two frequently-used additives, CN and DIO, have profound effects on the UV-Vis absorption of BTIC-CF_3-m film and their effects are quite different. The UV-Vis absorption spectra of neat BTIC-CF_3-m films with and without

additives were measured and the corresponding profiles are shown in **Figure 1**c, in which the profiles were normalized against the peaks at ~840 nm. It can be observed that the absorption profile of pristine film shows a triplet, at 660, 728 and 836 nm, which indicated that H- and J-aggregation are coexisting. These three peaks represent H-aggregation, monomer and J-aggregation, respectively.[23] The structures of the H-aggregated and J-aggregated states could also be observed from the single-crystal structure of BTIC-CF_3-γ, which is the main component of the BTIC-CF_3-m blend, as shown in **Figure 3**a and **Figure S3**. When the film is processed by CN, the absorption spectrum is blue-shifted by about 14 nm and the peak of H-aggregation obviously increased, indicating that the amount of H-aggregation is enhanced. In contrast, when the film is processed by DIO, the absorption spectrum is red-shifted by about 24 nm and the peak of H-aggregation decreases relatively, while the crystallinity increases substantially. This is confirmed by grazing incidence wide angle X-ray scattering (GIWAXS) data (see below). Combining the results of UV-Vis spectra and GIWAXS, it can be concluded that DIO is conducive to J-aggregation. The influence of additive concentration on molecular aggregation was also studied. As seen from **Figure 1**d, with the concentration of CN increases from 0 to 1%, the spectra are gradually blue-shifted. This blue shift ends when the J-aggregation peak shifts to 816 nm. In this process, the height of the J-aggregation peak gradually decreases, while the height of H-aggregation peak gradually increases. As shown in **Figure 1**e, when the concentration of DIO increases from 0 to 1%, the spectra are gradually red-shifted from 836 to 860 nm and the height of J-aggregation peak is gradually enhanced.

When BTIC-CF_3-m is blended with the polymer donor, PBDB-TF, the absorption spectrum of the corresponding pristine film is blue-shifted with the J-aggregation peak shifting to 816 nm (see **Figure 1**f), indicating that the addition of PBDB-TF is conducive to the formation of H-aggregation. According to our previous results, the addition of polymer could contribute to formation of H-aggregation in small molecules, perhaps because the polymer increased steric hindrance and restricted the molecular motion of small molecules, thus contributing to the formation of metastable H-aggregation.[29] Compared to the absorption spectrum of the pristine film, the spectrum of film processed by CN is not further blue-shifted, while that of film processed by DIO is red-shifted about 36 nm. It can be concluded that H- and J-aggregation coexist in BTIC-CF_3-m, and CN and DIO are conducive to the formation of H- and J-aggregation of BTIC-CF_3-m, respectively, in both neat BTIC-CF_3-m films and PBDB-TF:BTIC-CF3-m blend films. Beside BTIC-CF_3-m, it was found that H- and J-aggregation also coexist in many molecules as shown in **Figure S4, S5, S6, S7** and **S8**. Usage of additives is just one method to tune the aggregation types [27, 29-33] and the effect of the same additive on different molecules varies.

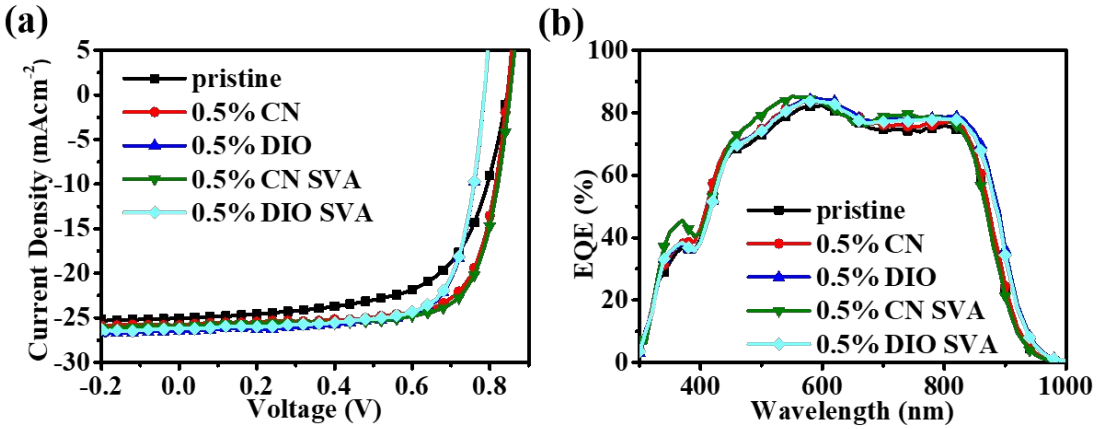

Figure 2. (a) *J-V* curves and (b) EQE of devices based on PBDB-TF:BTIC-CF_3-m under 100 mW cm^{-2} light illumination.

Table 1. Photovoltaic parameters of devices based on PBDB-TF:BTIC-CF_3-m under 100 mW cm^{-2} light illumination.

conditions	V_{oc} (V)	J_{sc} (mA cm^{-2})	J_{cal} (mA cm^{-2})	FF (%)	PCE (%)
pristine	0.84	25.03	23.94	63.57	13.37
	(0.84±0.01)	(24.81±0.35)		(63.03±0.67)	(13.22±0.21)
CN	0.84	25.82	24.58	73.19	15.87
	(0.84±0.01)	(25.46±0.41)		(72.55±0.79)	(15.61±0.32)
DIO	0.79	26.51	25.28	73.51	15.40
	(0.79±0.01)	(26.15±0.53)		(73.03±0.61)	(15.03±0.45)
CN SVA	0.85	25.98	24.76	74.06	16.36
	(0.84±0.01)	(25.62±0.39)		(73.45±0.74)	(16.11±0.31)
DIO SVA	0.79	26.26	25.02	73.17	15.18
	(0.79±0.01)	(25.97±0.42)		(72.78±0.58)	(14.92±0.43)

Average value ± standard deviation were from the statistics of 20 different devices.

Since aggregation type has such a distinct influence on light absorption in this system, and is a key factor in the performance of OSCs, corresponding devices were

fabricated with the structure of ITO/ZnO/PBDB-TF:BTIC-CF3-m/MoO_x/Ag and their photovoltaic performances were measured. It was found that both DIO and CN could efficiently improve the PCE of the devices based on PBDB-TF:BTIC-CF3-m blend. However, the two additives had very different influences on V_{oc} and J_{sc} as shown in **Figure 2**a. The detailed parameters are listed in **Table 1**. It was observed that CN could keep the high V_{oc} of 0.84 V and improve the J_{sc} from 25.03 mA cm^{-2} to 25.82 mA cm^{-2}, compared to the pristine device. In contrast, DIO decreased the V_{oc} sharply from 0.84 V to 0.79 V, while increasing the J_{sc} more efficiently to 26.51 mA cm^{-2}. The external quantum efficiency (EQE) curves show that the onset of EQE of device processed by DIO is red-shifted (**Figure 2**b), while that of device processed by CN does not change, which is consistent with the absorption spectra. Compared to that of a device processed by CN, the extra enhancement of the J_{sc} of device processed by DIO comes mainly from the improvement of EQE from 700 nm to 960 nm, which is the absorption range of J-aggregation. Therefore, the improvement of J-aggregation is the prime reason for the higher J_{sc} of devices processed by DIO.

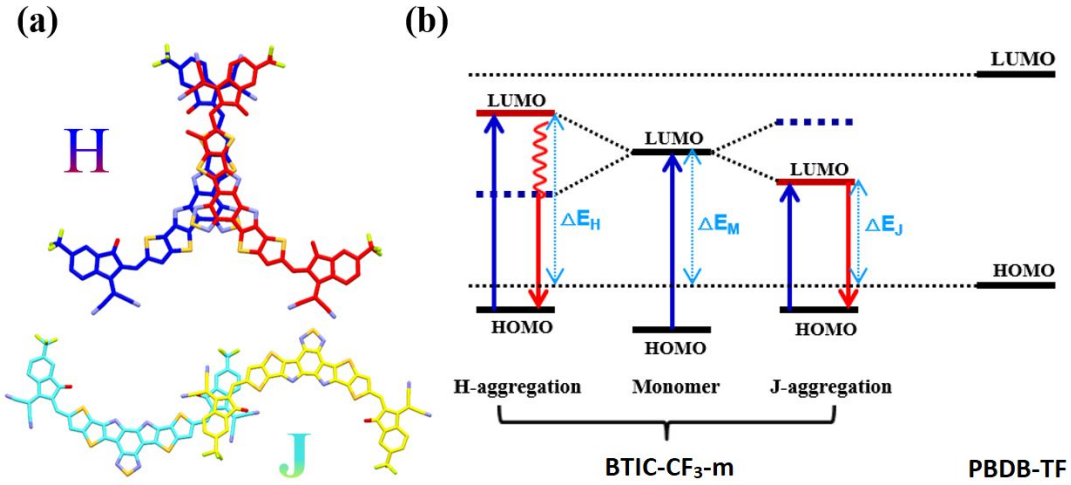

Figure 3. (a) The stacking structures of H- and J-aggregation of BTIC-CF_3-γ, (b) Scheme of the energy levels of H- and J-aggregation of BTIC-CF_3-m and PBDB-TF.

H- and J-aggregation also have deep and different influences on the electronic energy levels, which is key to the V_{oc} of the corresponding OSCs. The scheme of the electronic energy levels of H- and J-aggregation is shown in **Figure 3**b. Due to the π–π interactions between adjacent conjugated units, the corresponding lowest excited level splits into two.[20] For H-aggregation, the splitting is larger than J-aggregation due to the stronger coupling interaction resulted from the larger area of π-π overlap (see **Figure 3**a). After excitation, electrons in ground state of H-aggregation will move to the higher excited energy level, while those of J- aggregation will move to the lower excited energy level.[34] These two excited energy levels are the actual LUMO energy levels of H- and J-aggregation. The band gap between the LUMO energy level of the acceptor and the HOMO energy level of the donor determines the V_{oc} of the OSC device. Therefore, H-aggregation of acceptor can improve the V_{oc}, which explains that a device processed by CN has a higher V_{oc} than one processed by DIO. From another

point of view, the lower LUMO energy level of J-aggregation leads to the electrons in ground state of J-aggregation being excited more easily, which supports production of excitons and consequently a larger J_{sc}.

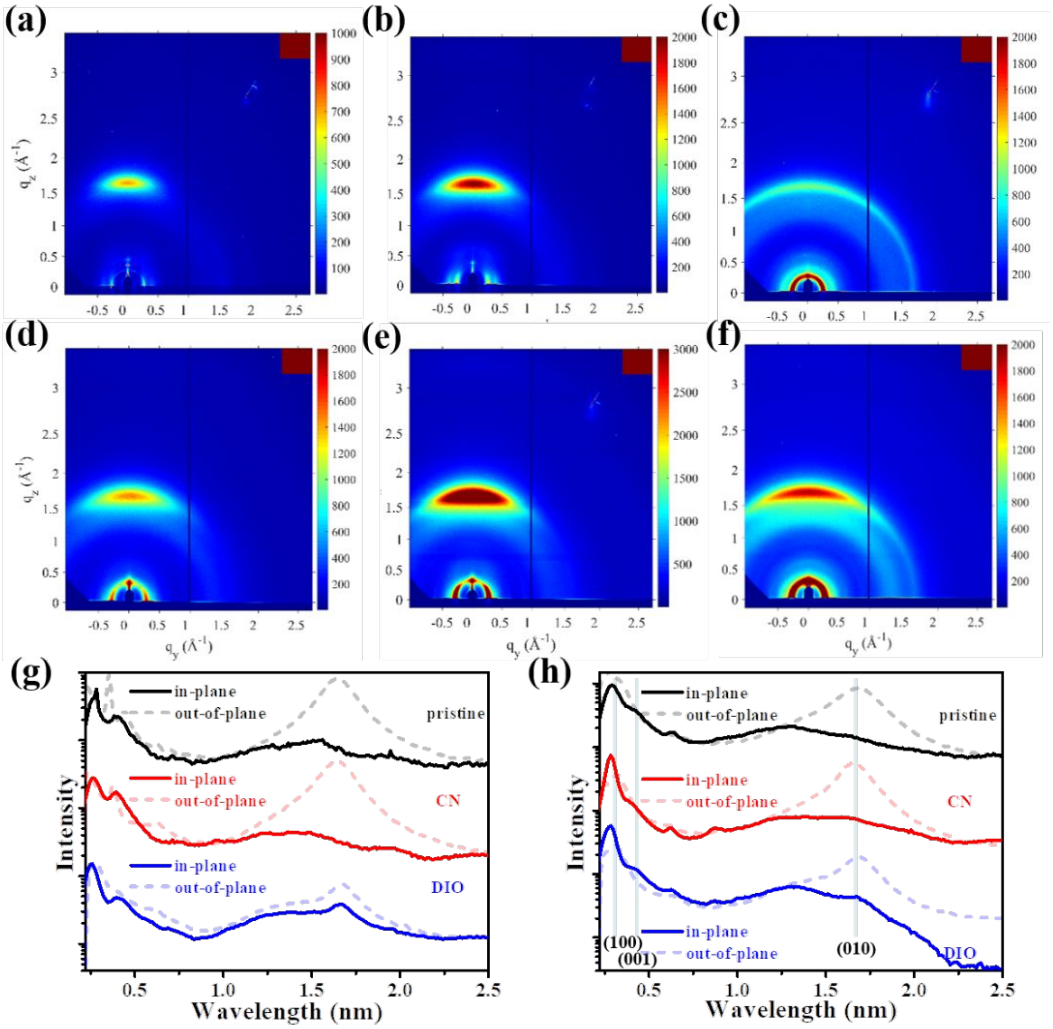

Figure 4. Two-dimensional GIWAXS patterns of neat BTIC-CF_3-m films (a) without additive, (b) with CN and (c) DIO and (g) the corresponding cut-line profiles; Two-dimensional GIWAXS patterns of blend PBDB-TF:BTIC-CF_3-m films (d) without additive, (e) with CN and (f) DIO and (h) the corresponding cut-line profiles.

Table 2. Characteristic length scale of packing phenomenon for BTIC-CF_3-m in blend film of PBDB-TF:BTIC-CF3-m.

	(100)			(001)			(010)		
	Distance[a] [Å]	FWHM[b] [$Å^{-1}$]	CCL[c] [Å]	Distance[a] [Å]	FWHM[b] [$Å^{-1}$]	CCL[c] [Å]	Distance[a] [Å]	FWHM[b] [$Å^{-1}$]	CCL[c] [Å]
pristine	21.96	0.083	75.66	16.57	0.198	31.72	3.72	0.281	22.35
CN	22.67	0.080	78.50	15.70	0.114	55.01	3.72	0.227	27.67
DIO	22.19	0.055	114.2	16.80	0.208	30.19	3.77	0.229	27.42

[a] distance represents packing distance; [b] FWHM represents full-width at half maximum; [c] CCL represents crystal coherence length.

More measurements were carried out to further understand the reasons for the different performance of devices processed by CN and DIO. To investigate the molecular packing, grazing incidence wide-angle X-ray scattering (GIWAXS) was carried out and the results are shown in **Figure 4**. The molecules in pristine BTIC-CF_3-m film are mainly face-on oriented with low crystallinity, as seen in **Figure 4**a. Both the additives CN and DIO can improve the crystallinity, but CN is much more effective, as seen in **Figure 4**b, 4c and 4g. The BTIC-CF_3-m molecules processed by 0.5% (v/v) DIO partly become randomly oriented, while those processed with 0.5% (v/v) CN mainly still remain face-on. The influence of CN and DIO in blend films of PBDB-TF:BTIC-CF_3-m is similar to that in neat BTIC-CF_3-m films as shown in **Figures 4**d, 4(e), 4(f) and 4 (h). The key parameters for the packing behavior of the blend films were calculated [35-36] and are summarized in **Table 2**. The

crystal coherence length (CCL) of π-π stacking along the (010) direction, which was calculated from the out-of-plane cut-line profiles, had an increase of similar magnitude from 22.35 Å to 27.42 Å or 27.67 Å for films processed by CN and DIO, respectively. However, the CCL values along the (100) and (001) directions, calculated from the in-plane cut-line profiles, are very different. The CCL of film processed by DIO along the (001) direction increased greatly, from 31.72 Å to 55.01 Å, while the CCL of film processed by CN was only 30.19 Å. In contrast, the CCL along the (100) direction of film processed by CN increased sharply from 75.66 Å to 114.2 Å, while that of film processed by DIO only increased to 78.50 Å. This phenomenon may be attributed to the difference of H-/J-aggregation in BTIC-CF_3-m. According to the above discussion, H- and J-aggregation coexist in BTIC-CF_3-m, and CN and DIO contribute to the formation of H- and J-aggregation of BTIC-CF_3-m, respectively. However, the integrated CCLs of films processed by CN and DIO are on the whole, similar, although the sizes along different directions vary.

Crystallinity and molecular orientation are both key to the mobility of charge carriers. The charge carrier mobilities were measured by a space charge-limited current (SCLC) method. Electron-only and hole-only devices based on PBDB-TF:BTIC-CF_3-m were fabricated and the corresponding *J-V* curves are shown in **Figure 5**a and 5b, respectively. The electron mobility (μ_e) and hole mobility (μ_h) were calculated and the results are listed in **Table 3**. These results show that the addition of CN and DIO improve the electron mobility from 1.9×10^{-5} cm^2 V^{-1} s^{-1} to 8.1×10^{-5} cm^2 V^{-1} s^{-1} and 3.5×10^{-5} cm^2 V^{-1} s^{-1}, respectively. The hole mobilities are

similar and are 9.0×10^{-5} cm^2 V^{-1} s^{-1}, 1.2×10^{-4} cm^2 V^{-1} s^{-1} and 1.0×10^{-4} cm^2 V^{-1} s^{-1} for pristine film and films processed by CN and DIO, respectively. As a result, the ratios of μ_h/μ_e are 4.7, 1.5 and 2.9 for pristine film and films processed by CN and DIO, respectively. It is observed that both the two additives can enhance electron mobility. This is due to the improvement of crystallinity, which is confirmed by the GIWAXS data. Specifically, the CN additive improves the electron mobility more effectively than DIO and the charge carrier mobilities are more balanced in the film processed by CN. The reason for the higher electron mobility of films processed by CN may be the improvement of H-aggregation with large overlap of π-π stacking combined with face-on orientation.[16, 32]

Table 3. The summary of charge mobility, P(E,T) and σ of devices based on PBDB-TF:BTIC-CF_3-m.

	pristine	**0.5% CN**	**0.5% DIO**
μ_e (cm^2 V^{-1} s^{-1})	1.9×10^{-5}	8.1×10^{-5}	3.5×10^{-5}
μ_h (cm^2 V^{-1} s^{-1})	9.0×10^{-5}	1.2×10^{-4}	1.0×10^{-4}
μ_h/μ_e	4.7	1.5	2.9
P(E,T) (%)	99.4	99.7	99.9
σ	0.930	0.944	0.964

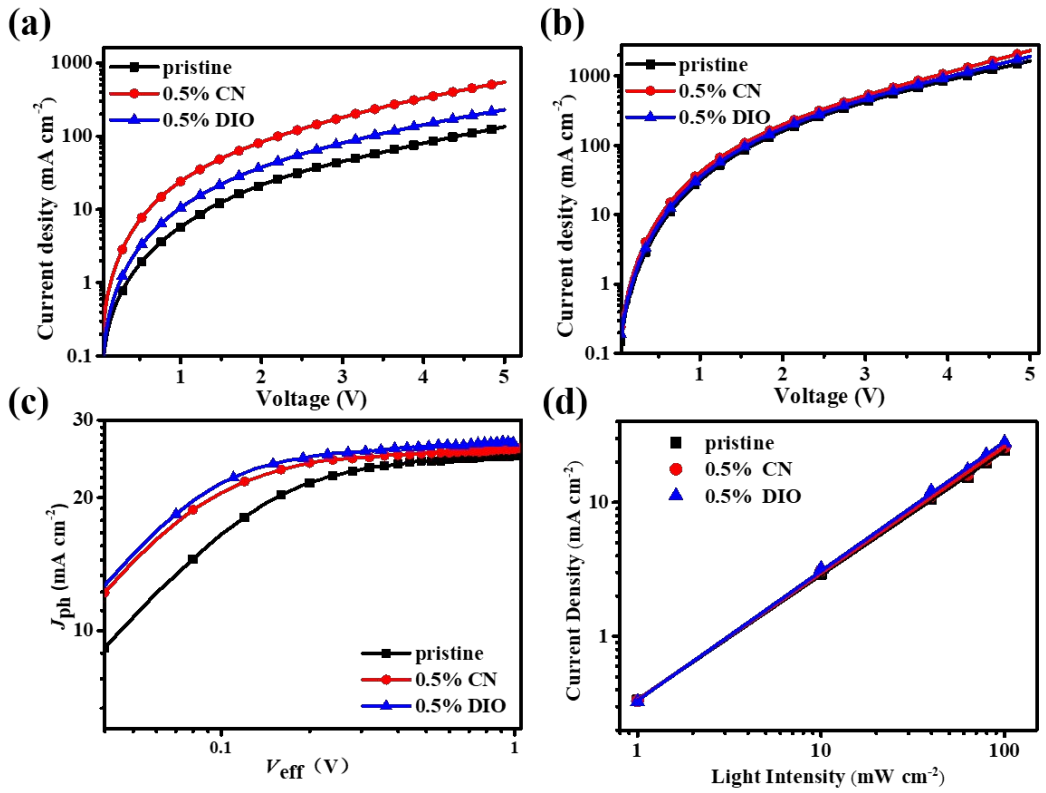

Figure 5. Dark $J-V$ curves of (a) electron-only and (b) hole-only devices based on PBDB-TF:BTIC-CF_3-m; (c) $J_{ph}-V_{eff}$ curves of devices based on PBDB-TF:BTIC-CF_3-m; (d) light intensity dependent J_{sc} of devices based on PBDB-TF:BTIC-CF_3-m.

The impact of the addition of CN and DIO on the exciton dissociation probability (P(E,T)) was also investigated. The relationship between the photocurrent density (J_{ph}) and the effective voltage (V_{eff}) is shown in **Figure 5**c. The saturation current density (J_{sat}) will be decided only by the maximum exciton generation rate, assuming that all of the photogenerated excitons are dissociated under high V_{eff}. P(E,T) is determined by the ratio J_{ph}/J_{sat}.[37] The J_{sat} of the three devices are 25.19 mA cm^{-2} (pristine device), 25.90 mA cm^{-2} (device processed by CN) and 26.53 mA cm^{-2} (device processed by DIO), respectively. Therefore, the calculated P(E,T) values in the short-circuit condition are 99.4%, 99.7% and 99.9% for the pristine device and

devices processed by CN and DIO, respectively. These three high values of P(E,T) indicate that all the three devices have enough driving force to separate the excitons at the interfaces between donor and acceptor in the short-circuit condition. The bimolecular recombination was investigated by measuring J_{sc} under different light intensities. J_{sc} and light intensities (P_{light}) follow a relationship, described as $J_{sc} \propto P_{light}^{\sigma}$. According to **Figure 5**d, the exponential factors (σ) of the pristine device and the devices processed by CN and DIO were calculated and the values are 0.930, 0.944 and 0.964, respectively. The results show that both CN and DIO can reduce bimolecular recombination, but DIO is more effective.

Nanoscale morphology is also a key factor in the performance of OSCs and was measured by atomic force microscopy (AFM) and transmission electron microscopy (TEM). As shown in **Figure S9** and **Figure S10**, the three active layers have similar morphology and surface roughness. The photoluminescence (PL) spectra were obtained and are shown in **Figure S11**. It can be seen that the neat BTIC-CF_3-m film has two fluorescence peaks. However, all of the three fluorescence spectra of the blend films of PBDB-TF:BTIC-CF3-m with or without additives fail to show any peaks, indicating that the phase separation sizes of the three films allow almost all of the excitons to diffuse into the interface between donor and acceptor. Combined with the CCLs calculated from GIWAXS, use of CN or DIO can enlarge the phase separation sizes and the sizes will not be excessively sized.

According to the above discussion, both H- and J-aggregation can enhance the PCE in this system. We tried to further improve the amount of aggregation in the PBDB-TF:BTIC-CF3-m blend film with CN additive by SVA. The film was set in methylene chloride (CH_2Cl_2) vapor for 5 s, which has been reported to tune H- and J-aggregation efficiently.[33] This improved the J_{sc} and FF to 25.98 mA cm^{-2} and 74.06%, respectively, and consequently a further enhanced PCE of 16.36%. In order to find the reason of the enhancement, some measurements were carried out. From **Figure S12**, it can be observed that SVA fine-tuned the spectrum with slight improvement of the J-aggregation peak. It's hard to discuss the change of H-aggregation peak because it overlaps with the absorbance of PBDB-TF. The charge mobility, P(E,T) and σ of devices based on PBDB-TF:BTIC-CF3-m blend with CN after SVA were also measured as shown in **Figure S13**, **Figure S14**, **Figure S15**. Compared to that before SVA, charge mobility was improved with μ_h and μ_e enhanced to 2.1×10^{-4} cm^2 V^{-1} s^{-1} and 1.6×10^{-4} cm^2 V^{-1} s^{-1}, respectively. P(E,T) was slightly decreased from 99.7% to 99.4%, while σ was essentially unchanged with the value of 0.945. Therefore, the improvement of PCE by SVA is a comprehensive result.

Conclusions

In summary, it is found that H- and J-aggregation coexist in BTIC-CF_3 and they can be easily controlled by different additive, which offers us an opportunity to study systematically the role of the two types of aggregation by directly comparing their

effect on various photovoltaic performance parameters in one system. Two common additives, CN and DIO, are found to be conducive to the formation of H- and J-aggregation, respectively. H-aggregation favors higher V_{oc} due to a higher lowest excited energy level, while J-aggregation contributes to higher J_{sc} because of extended absorption range and a lower energy needed to excite the J-aggregation. Both of the two aggregations can improve the FF. As a result, both the two additives are found to enhance the PCE. However, the device with DIO as additive has a little lower PCE due to the substantial reduction of $V_{oc.}$ By the means of SVA to further improve the H- and J-aggregation of BTIC-CF3-m in active layer with CN as additive, the PCE is further enhanced to 16.36%. From this work, it can be reasonably speculated that, under the premise of the similar nanoscale morphology, which is key to FF, PCE is decided by the balance of V_{oc} and J_{sc}, which can be tuned by H- and J-aggregation for acceptor materials. This work provides us with a better and deeper understanding of OSCs and offers us a new perspective with which to precisely regulate the morphology of the active layer, which includes not only phase separated sizes but also aggregation type, to better improve the performance of OSCs in a targeted way.

Conflicts of interest

There are no conflicts to declare.

Acknowledgements

This work was financially supported by the China Postdoctoral Science Foundation (2019M651639), the National Natural Science Foundation of China (21733005, 51903116, and 21975115), Shenzhen Fundamental Research program (JCYJ2019080916301, JCYJ20170817111214740 and KQJSCX20180319114442157), Guangdong Provincial Key Laboratory of Catalysis (2020B121201002), Guangdong Innovative and Entrepreneurial Research Team Program (2016ZT06G587) and Shenzhen Sci-Tech Fund (KYTDPT20181011104007). We thank Dr. Joseph Strzalka and Dr. Zhang Jiang for the assistance with GIWAXS measurements. Use of the Advanced Photon Source (APS) at the Argonne National Laboratory was supported by the U.S. Department of Energy, Office of Science, Office of Basic Energy Sciences, under contract No. DE-AC02-06CH11357. We also thank the SUSTech Core Research Facilities for the AFM and TEM measurements.

References

1. Y. Lin, J. Wang, Z. G. Zhang, H. Bai, Y. Li, D. Zhu and X. Zhan, *Adv. Mater.,* 2015, **27**, 1170-1174.
2. Z. Xiao, X. Jia, D. Li, S. Wang, X. Geng, F. Liu, J. Chen, S. Yang, T. P. Russell and L. Ding, *Sci. Bull.,* 2017, **62**, 1494-1496.
3. J. Yuan, Y. Zhang, L. Zhou, G. Zhang, H.-L. Yip, T.-K. Lau, X. Lu, C. Zhu, H. Peng, P. A. Johnson, M. Leclerc, Y. Cao, J. Ulanski, Y. Li and Y. Zou, *Joule,* 2019, **3**, 1-12.

4. Q. Liu, Y. Jiang, K. Jin, J. Qin, J. Xu, W. Li, J. Xiong, J. Liu, Z. Xiao, K. Sun, S. Yang, X. Zhang and L. Ding, *Sci. Bull.,* 2020, **65**, 272-275.

5. L. Meng, Y. Zhang, X. Wan, C. Li, X. Zhang, Y. Wang, X. Ke, Z. Xiao, L. Ding, R. Xia, H.-L. Yip, Y. Cao and Y. Chen, *Science,* 2018, **361**, 1094-1098.

6. T. Yan, W. Song, J. Huang, R. Peng, L. Huang and Z. Ge, *Adv. Mater.,* 2019, **31**, 1902210.

7. H. Bin, Z. G. Zhang, L. Gao, S. Chen, L. Zhong, L. Xue, C. Yang and Y. Li, *J. Am. Chem. Soc.,* 2016, **138**, 4657-4664.

8. Y. Cui, H. Yao, J. Zhang, T. Zhang, Y. Wang, L. Hong, K. Xian, B. Xu, S. Zhang, J. Peng, Z. Wei, F. Gao and J. Hou, *Nat. Commun.,* 2019, **10**, 2515.

9. L. Hong, H. Yao, Z. Wu, Y. Cui, T. Zhang, Y. Xu, R. Yu, Q. Liao, B. Gao, K. Xian, H. Y. Woo, Z. Ge and J. Hou, *Adv. Mater.,* 2019, **31**,1903441.

10. X. Xu, K. Feng, Z. Bi, W. Ma, G. Zhang and Q. Peng, *Adv. Mater.,* 2019, **31**, 1901872.

11. M. Más-Montoya and R. A. J. Janssen, *Adv. Funct. Mater.,* 2017, **27**, 1605779.

12. D. Yan, W. Liu, J. Yao and C. Zhan, *Adv. Energy Mater.,* 2018, **8**, 1800204.

13. J. Shin, N. S. Kang, K. H. Kim, T. W. Lee, J. I. Jin, M. Kim, K. Lee, B. K. Ju, J. M. Hong and D. H. Choi, *Chem. Commun. (Camb),* 2012, **48**, 8490-8492.

14. M. Schulz, M. Mack, O. Kolloge, A. Lutzen and M. Schiek, *Phys. Chem. Chem. Phys.,* 2017, **19**, 6996-7008.

15. K. Cai, J. Xie, D. Zhang, W. Shi, Q. Yan and D. Zhao, *J. Am. Chem. Soc.,* 2018, **140**, 5764-5773.

16. O. J. Dautel, G. Wantz, R. Almairac, D. Flot, L. Hirsch, J.-P. Lere-Porte, J.-P. Parneix, F. Serein-Spirau, L. Vignau and J. J. E. Moreau, *J. Am. Chem. Soc.,* 2006, **128**, 4892-4901.

17. G. Chen, H. Sasabe, Y. Sasaki, H. Katagiri, X.-F. Wang, T. Sano, Z. Hong, Y. Yang and J. Kido, *Chem. Mater.,* 2014, **26**, 1356-1364.

18. T. P. Martin, A. J. Wise, E. Busby, J. Gao, J. D. Roehling, M. J. Ford, D. S. Larsen, A. J. Moule and J. K. Grey, *J. Phys. Chem. B,* 2013, **117**, 4478-4487.

19. T. Eder, T. Stangl, M. Gmelch, K. Remmerssen, D. Laux, S. Hoger, J. M. Lupton and J. Vogelsang, *Nat. Commun.,* 2017, **8**, 1641.

20. Y. Deng, W. Yuan, Z. Jia and G. Liu, *J. Phys. Chem. B,* 2014, **118**, 14536-45.

21. O. Ostroverkhova, *Chem. Rev.,* 2016, **116**, 13279-13412.

22. F. Würthner, C. Thalacker, S. Diele and C. Tschierske, *Chem. Eur. J.,* 2001, **7**, 2245-2253.

23. H. Menzel, B. Weichart, A. Schmidt, S. Paul, W. Knoll, J. Stumpe and T. Fischer, Langmuir, 1994, **10**, 1926-1933.

24. E. S. Emerson, M. A. Conlin, A. E. Rosenoff, K. S. Norland, H. Rodriguez, D. Chin and G. R. Bird, *J. Phys. Chem. C,* 1967, **71**, 2396-2403.

25. D. Chaudhuri, D. Li, Y. Che, E. Shafran, J. M. Gerton, L. Zang and J. M. Lupton, *Nano Lett.,* 2011, **11**, 488-492.

26. S. Verma, A. Ghosh, A. Das and H. N. Ghosh, *J. Phys. Chem. B,* 2010, **114**, 8327–8334.

27. Q. Zhao, J. Liu, H. Wang, M. Li, K. Zhou, H. Yang and Y. Han, *J. Mater. Chem. C,* 2015, **3**, 8183-8192.

28. H. Lai, Q. Zhao, Z. Chen, H. Chen, P. Chao, Y. Zhu, Y. Lang, N. Zhen, D. Mo, Y. Zhang and F. He, *Joule,* 2020, **4**, 688-700.

29. Q. Zhao, X. Yu, Z. Xie, J. Liu and Y. Han, *ACS Appl. Energ. Mater.,* 2018, **1**, 6338-6344.

30. J. Kim, K.-J. Baeg, D. Khim, D. T. James, J.-S. Kim, B. Lim, J.-M. Yun, H.-G. Jeong, P. S. K. Amegadze, Y.-Y. Noh and D.-Y. Kim, *Chem. Mater.,* 2013, **25**, 1572-1583.

31. M.-H. Yoon, A. Facchetti, C. E. Stern and T. J. Marks, *J. Am. Chem. Soc.,* 2006, **128**, 5792-5801.

32. S.-o. Kim, T. K. An, J. Chen, I. Kang, S. H. Kang, D. S. Chung, C. E. Park, Y.-H. Kim and S.-K. Kwon, *Adv. Funct. Mater.,* 2011, **21**, 1616-1623.

33. Q. Zhao, X. Yu, J. Liu, Z. Xie and Y. Han, *Org. Electron.,* 2016, **37**, 6-13.

34. F. C. Spano, *Accounts Chem. Res.,* 2010, **43**, 429-439.

35. J. Rivnay, S. C. Mannsfeld, C. E. Miller, A. Salleo and M. F. Toney, *Chem. Rev.,* 2012, **112**, 5488-5519.

36. S. Pang, R. Zhang, C. Duan, S. Zhang, X. Gu, X. Liu, F. Huang and Y. Cao, *Adv. Energ. Mater.,* 2019, **9**, 1901740.

37. L. Lu, W. Chen, T. Xu and L. Yu, *Nat. Commun.,* 2015, **6**, 7327.